# TOWARD SMART CONTROL OF SEPARATION AROUND A WING
## -An Evaluation System of Flow Drags and Control Devices-

Takehiko Segawa, Hiroyuki Abe, Yoshihiro Kikushima, and Hiro Yoshida
National Institute of Advanced Industrial Science and Technology
1-2-1 Namiki, Tsukuba 305-8564, Japan

Akira Nishizawa and Shohei Takagi
National Aerospace Laboratory of Japan
Chofu, Tokyo 182-8522, Japan

**Abstract**

In order to evaluate reactive flow-control devices, direct measurement of skin frictional drag in laminar and turbulent flows was carried out using the fiber Bragg grating system. By using two FBG sensors for obtaining stain measurements and one for monitoring temperature fluctuations, it is possible to accurately evaluate skin friction coefficients that are close to the values obtained by using a load cell. The FBG system with higher time resolution can determine the optimal control method of the turbulent flow and reveal the mechanism of drag reduction by reactive turbulence control.

## 1. Introduction

Near-wall streamwise vortices such as low-speed streaks are the main source of turbulence production and, consequently, increase in drag. In the last decade, besides the passive methods like riblets and LEBU[1,2], reactive turbulence control methods to reduce the skin frictional drag have been the subject of numerous studies. Reactive control methods have attracted attention in a wide variety of fields ranging from the retardation of the laminar to turbulent boundary layer transition to the regulation of the fully developed turbulent boundary layer. A previous study showed that selective suction through many holes or slots in the wall effectively delays the breakdown of the low-speed region and consequently reduces the production of turbulent energy near the wall[3]. Recently, interactions between low-speed coherent structures and artificial disturbances were also observed in a fully developed turbulent flow in a closed loop water channel[4]. In the experiment, artificial disturbances were produced by a series of oscillating piezo-ceramic actuators arranged in the wall in the spanwise direction. The low-speed structures generated by the actuator array interacted with the longitudinal vortices and inhibited the construction of coherent structures in the vicinity of the wall. Furthermore, a number of studies for reactive control of laminar and turbulent flows have been carried out experimentally and numerically using suction and blowing, which are generated by micro electro-mechanical systems (MEMS) (see, for example, references [5] and [6]).

On the other hand, the measurement of skin frictional drag is important for evaluating the effect of reactive control of turbulence. The Preston tube is a tool for measuring skin friction[7], but this method is not suitable for flows with larger drag fluctuations due to its poor time resolution. Load cells and strain gauges are also useful tools for measuring the skin frictional drag of a separated and floating plate in a channel. Although those methods can be utilized to measure the total skin friction of the floating plate directly, the strain gauges are generally fragile and their output signals are strongly

influenced by fluctuations in the surrounding temperature. In addition, since the dynamic range of the load cells is relatively narrow, the suitable cell applicable to each measurement should be determined. Hence, a more convenient method of measuring drag that is robust and has high time resolution is required.

Using the fiber Bragg grating (FBG) system, we evaluated real-time variations of skin frictional drag induced by several reactive turbulence control methods. The present FBG sensor has a larger dynamic range of 0.1 mN to 30 N and shows strong linearity. The output signal of the FBG sensor has two components: strain and temperature. Both contributions to the output signal can be clearly separated by using two FBG sensors. The present study is the first attempt to apply the FBG system to fluid dynamic experiments, i.e. the evaluation of the reactive control of turbulence.

## 2. Experimental Setup

The FBG system (NTT, FBG-IS) with three detecting elements (A, B, and C) is shown in Fig. 1. A closed loop water channel with a 1,700×396×315 $mm^3$ test section was used. The free stream velocity varied from $U_\infty$ = 0.1 to 0.5 m/s. The 10 mm long FBG sensor with two thousand gratings was set at the designed spacing in order to distinguish it from the other sensors. The broadband laser light with a wavelength ranging from 1528 to 1568 nm travels through an optical fiber 125 μm in diameter. When the FBG sensor is strained by external forces, the light with the wavelength corresponding to Bragg's wavelength ($\lambda_B$) is reflected from each sensor following the relationship:

$$\lambda_B = 2n_0\Lambda, \qquad (1)$$

where $n_0$ is the averaged refractive index in a fiber sensor and Λ is the grating interval. As shown in Fig. 1(b), three sensors are mounted in different locations in $L$ = 300 mm long floating flat plate, which is suspended by four stainless steel wires 0.3 mm in diameter and set in the 1300 mm long steady plate of the channel. Actuator arrays for reactive control of turbulence are placed in the upstream of the floating plate, shown as the darker area in Fig. 1.

Generally, the FBG sensor has been widely used in the strain measurement of various structures and elements because of its easily distributed installment[8]. In the present study, two detectors, i.e. sensors A and B in Fig. 1(a), are used as strain sensors to precisely measure frictional drag in the downstream of the actuator array. They are suspended between the fixed plate and floating plate.
The remaining sensor, C, is used for compensation of the temperature drift of the FBG system, which is extremely sensitive to temperature change as well as the mechanical strain. Figure 2 shows the wavelength shifts of the three sensors in response to the temperature changes. From Fig. 2, we find that the present sensors stretch 0.01 nm/K. By using Sensor C, it is possible to minimize the effect of the temperature drift on the skin frictional drag. As a result, accuracy of the skin friction measurement is improved to as high as $10^{-3}$ N (Fig. 3). The dynamic response of the present FBG system is higher than 40 Hz.

In order to measure the skin friction coefficient of the air by using the FBG system, a wind tunnel with a 2,000×500×1,000 $mm^3$ test section was used. The free stream velocity is variable, ranging from $U_\infty$ = 2.5 to 12.5 m/s. The contraction ratio of the duct cross sections is 8:1. The architecture of the measurement system is the same as that of the channel.

## 3. Experimental Results

### 3.1 Measurement of Skin Friction Drags

The local skin friction coefficient, $C_f$, in the floating plate in the air and the water was analyzed from the data acquired by the FBG sensors. In order to compare $C_f$ with the total skin friction coefficient of the entire flat plate, we introduce a corrected skin friction coefficient, $C_f^*$, which is

equivalent to the total skin friction coefficient. $C_f^*$ is defined as:

$$C_f{}^* = (1-\gamma)C_{fL} + \gamma C_{fT}, \tag{2}$$

where $\gamma$ is the intermittency factor introduced by by Dhawan and Narasimha[9]. $C_{fL}$ and $C_{fT}$ are the corrected total skin friction coefficients of laminar and fully developed turbulent flow[10], which are defined as follows:

$$C_{fT} = \frac{C_f}{\frac{x}{L} + 1 - \frac{x}{L}\left(\frac{x}{x+L}\right)^{-0.2}}, \tag{3}$$

$$C_{fL} = \frac{C_f}{\frac{x}{L} + 1 - \left(\left(\frac{x}{L}\right)^2 + \frac{x}{L}\right)^{0.5}}, \tag{4}$$

where $x$ is the distance from the entrance of tunnel. Figure 4 shows $C_f^*$ as a function of the Reynolds number, $Re_L = U_\infty(x + L)/\nu$, in the wind tunnel test. In a lower $Re_L$, $C_f^*$ decreases along the dotted line, which corresponds to $C_f^* \sim Re_L^{-1/2}$. At higher $Re_L$, it separates from the line. Therefore, it was found that the air flow tends from laminar to turbulent flow. While in the water channel tests, as can be seen in Fig. 5, $C_f^*$ changes according to $Re_L^{-1/5}$. This result implies that the flow is under fully developed turbulence over the entire $Re_L$ regime measured in this study. By using the FBG system, the laminar-turbulent boundary layer transition behavior can be observed.

## 3.2 Drag Variations by Roughness Elements

As a first step of evaluating drag variations caused by reactive turbulence control, some roughness elements were used instead of the actuators. 13 balls with 15 mm diameter were used as the elements. The elements were placed spanwise on the wall at the entrance of the wind tunnel test section. The spacing of the balls was 30 mm. By creating perturbations in the vicinity of the flat plate, the laminar boundary layer tends to the turbulent boundary layer. Figure 6 shows the strain as a function of the free stream velocity in the wind tunnel. Over the entire range observed, the strain increases due to the development of the turbulent boundary layer. The shape factor at the center of the floating plate changes to $H_{12} = 1.4$, when the roughness elements are set on the plate, whereas $H_{12} = 2.6$ without the elements.

## 3.3 Drag Variations by Suction and Blowing

For a reactive turbulence control actuator, a suction-blowing type actuator array (Fig. 7) was tested. This actuator can generate horseshoe-like longitudinal vortices by water jets. There are 40 holes with $d = 1$ mm diameter in the stationary plate of the water channel. The water jets are discharged by two separate pistons, which are connected with two separate power amplifiers. By oscillating the two pistons with a phase difference of $180^o$ to each other, suction and blowing are generated alternately.

Figure 7(c) shows the flow pattern by the suction and blowing at the piston frequency of $f_p = 8$ Hz. The horseshoe-like longitudinal vortices are generated by a pair of suction-blowing holes. However, this flow state is unstable and becomes chaotic immediately, as shown in Fig. 7(d).

So far, remarkable changes of the flow pattern caused by the actuator have been observed actually. Regarding the drag changes relevant to such flow patterns, we have detected some drag reduction with the suction-blowing control by the FBG system in lower frequency of the piston, $f_p$, less than 5

Hz (Fig. 8). However, the mechanism of the drag reducing effects is still unclear. Therefore, we are now trying to see how the suction-blowing actuator effects on the near wall structure.

## 4. Concluding Remarks

Through the entire tests carried out here by using the wind tunnel and the water channel, we consider that the FBG system is a promising tool for precise measurements of minute skin friction variations. This is because we confirmed the following many advantages of the system: 1) First of all, since the FBG sensors are the optical ones, they are hardly influenced by the electromagnetic noises; 2) The sequential alignment of the sensors in one fiber extremely facilitates the signal data processing; 3) The raw output signal of the FBG system shows strong linearity against the temperature and the strain variations. This fact indicates that their simultaneous observation is possible; 4) The system has wide dynamic range compared to the conventional methods such as the Preston tube, and finally; 5) It has high robustness to the environment, i.e. durable under higher stresses and applicable to the measurements both in the air and in the water.

In the present study, we showed the feasibility of the FBG system for measurements of the frictional drag. In the future study, we will use the FBG sensor system for the measurements of various fluid dynamic forces, i.e. lifts. Application of the FBG system to the separation detector is one of the challenging topics.

## Acknowledgements

We sincerely thank Prof. H. Mizunuma and Mr. K. Murakami of Tokyo Metropolitan University for their kind advice and stimulating discussions. This research was carried out at the Center for Smart Control of Turbulence funded by MECSST of Japan.

## References

[1] Gad-el-Hak, M., *Flow Control: Passive, Active and Reactive Flow Management*, Cambridge University Press, London, 2000.

[2] Choi, K-S., "Turbulent drag-reduction mechanisms: strategies for turbulence management", *Turbulence Structure and Modulation*, CISM Course and Lectures 415, ed. A Soldati and R Monti, Springer, Wien, 161-212, 2001.

[3] Myose, R. Y. and Blackwelder, R. F., "Control of streamwise vortices using selective suction", AIAA J. **33**, 1076-1080, 1995.

[4] Segawa, T., Kawaguchi, Y., Kikushima, Y. and Yoshida, H., "Active control of coherent structures using an actuator array producing inclined wavy disturbances", J. Turbulence **3**, 015, 2002.

[5] Kerho, M., "Active reduction of skin friction drag using low-speed streak control", AIAA paper, 2002-0271, 2002.

[6] Lee, C. Y. and Goldstein, D. B., "Simulation of MEMS suction and blowing for turbulent boundary layer control", AIAA paper, 2002-2831, 2002.

[7] Zarbi, G. and Reynolds, A. J., "Skin friction measurements in turbulent flow by means of Preston tubes", Fluid Dyn. Res. **7**, 151-164, 1991.

[8] Rao, Y. J., "Recent progress in applications of in-fibre Bragg grating sensors", Optics and Lasers in Engineering **31**, 297-324, 1999.

[9] Dhawan, S. and Narasimha, R., "Some properties of boundary layer flow during the transition from laminar to turbulent motion", J. Fluid Mech. **3**, 418-437, 1958.

[10] Segawa, T., Abe, H., Kikushima, Y., Yoshida, H., and Mizunuma, H., "Measurement of turbulent skin frictional drag using a fiber Bragg grating system", AIAA paper, 2003-0646, 2003.

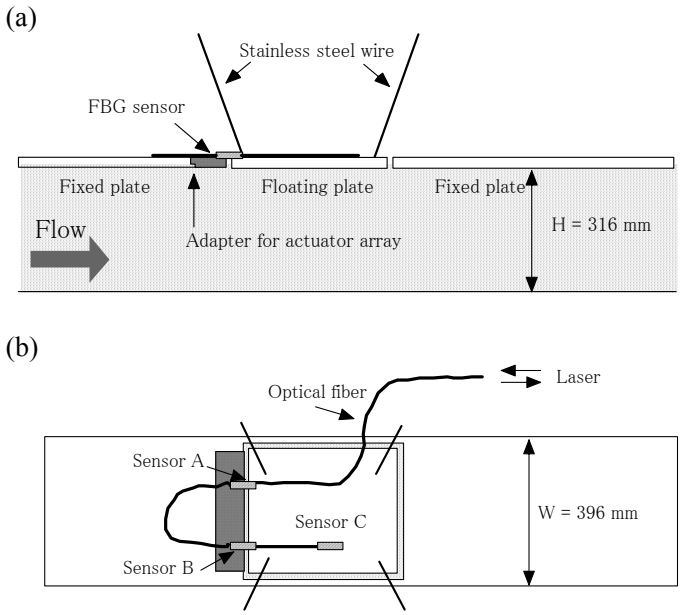


Figure 1 Schematic diagram of the FBG system for measurement of turbulent skin frictional drag. (a) Side view and (b) top view. The darker area indicates place in which the actuator array can be mounted.

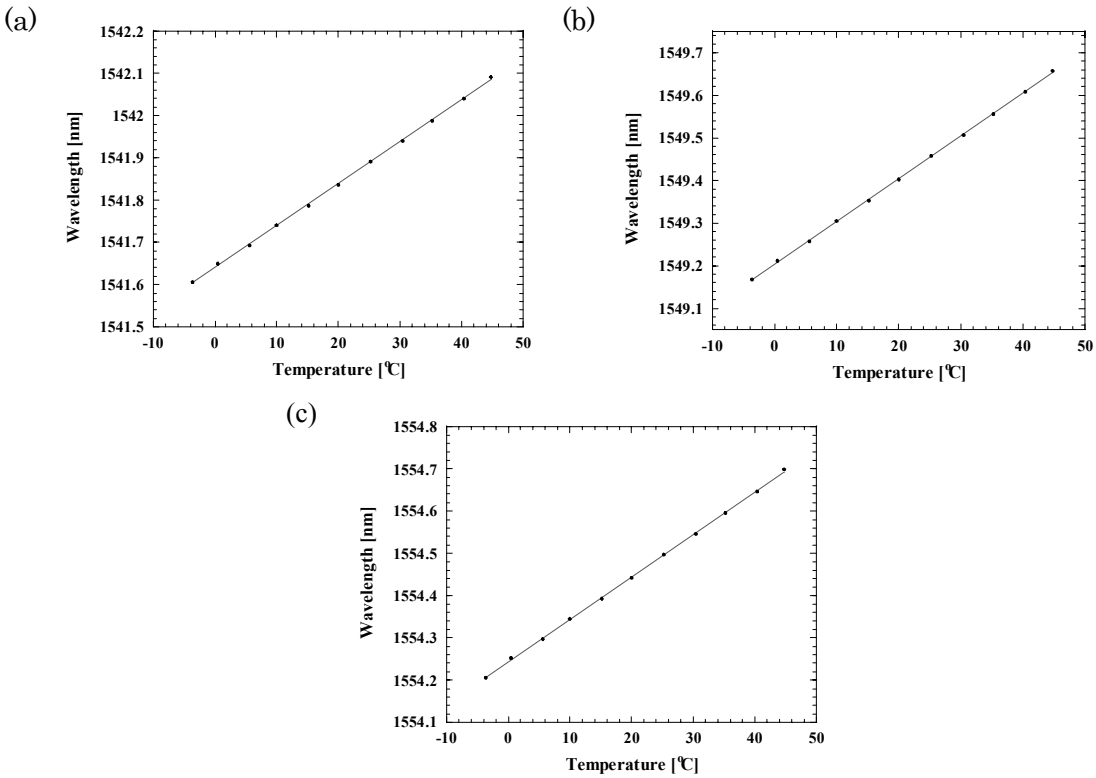


Figure 2 Measured Bragg's wavelength shifts of three sensors by temperature changes. The solid line shows the fitting by the linear function. (a) Sensor A; (b) Sensor B; and (c) Sensor C. Skin frictional drag can be analyzed from the signals of Sensors A and B. Sensor C is used for detecting the surrounding temperature.

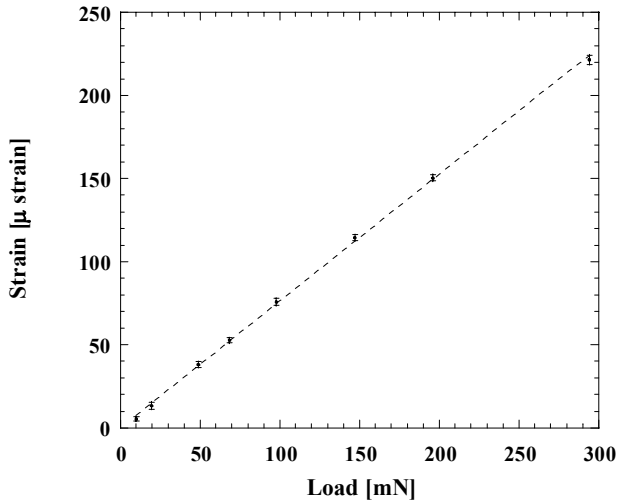


Figure 3 Strain vs. load in the floating plate measured by usig the FBG system in the wind tunnel.

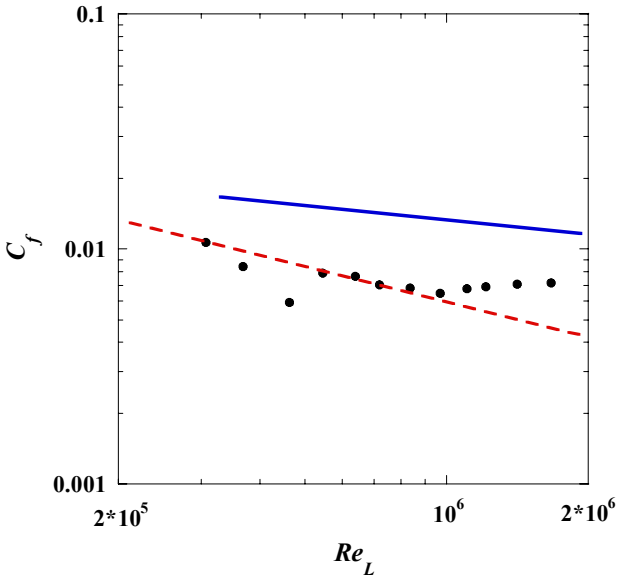


Figure 4 $C_f$ vs. $Re_L$ in the wind tunnel. The dotted line shows $C_f \sim Re_L^{-1/2}$ and the solid line shows $C_f \sim Re_L^{-1/5}$.

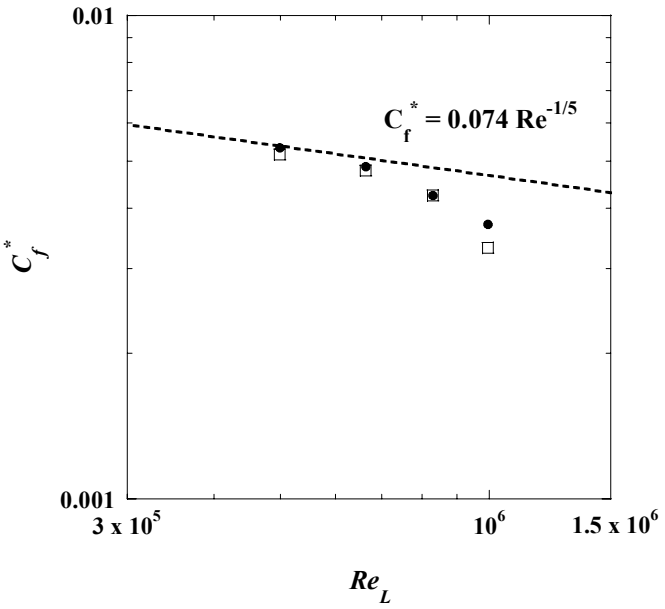


Figure 5 $C_f^*$ vs. $Re_L$ in the water channel. The dotted line shows $C_f^* = 0.074 Re_L^{-1/5}$. Solid and open symbols indicate $C_f^*$ measured by using the load cell and the FBG system respectively.

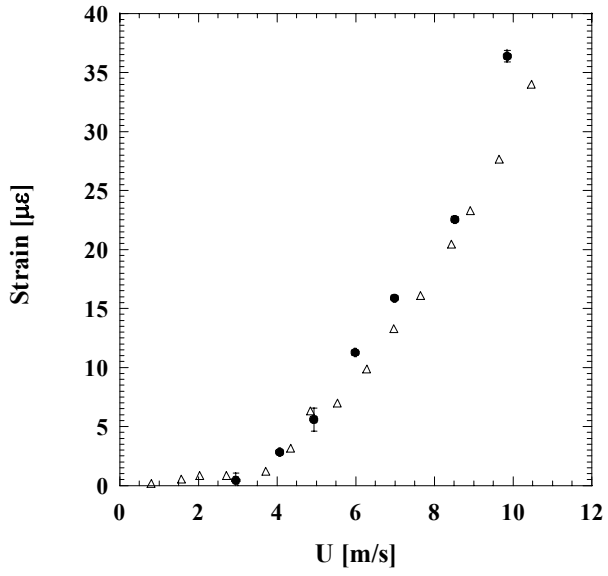


Figure 6 Strain vs. free stream velocity. At the entrance of the flat plate in the wind tunnel, the spherical roughness elements are set: Solid symbol is the strain without the roughness elements; Open symbol is the strain with roughness elements.

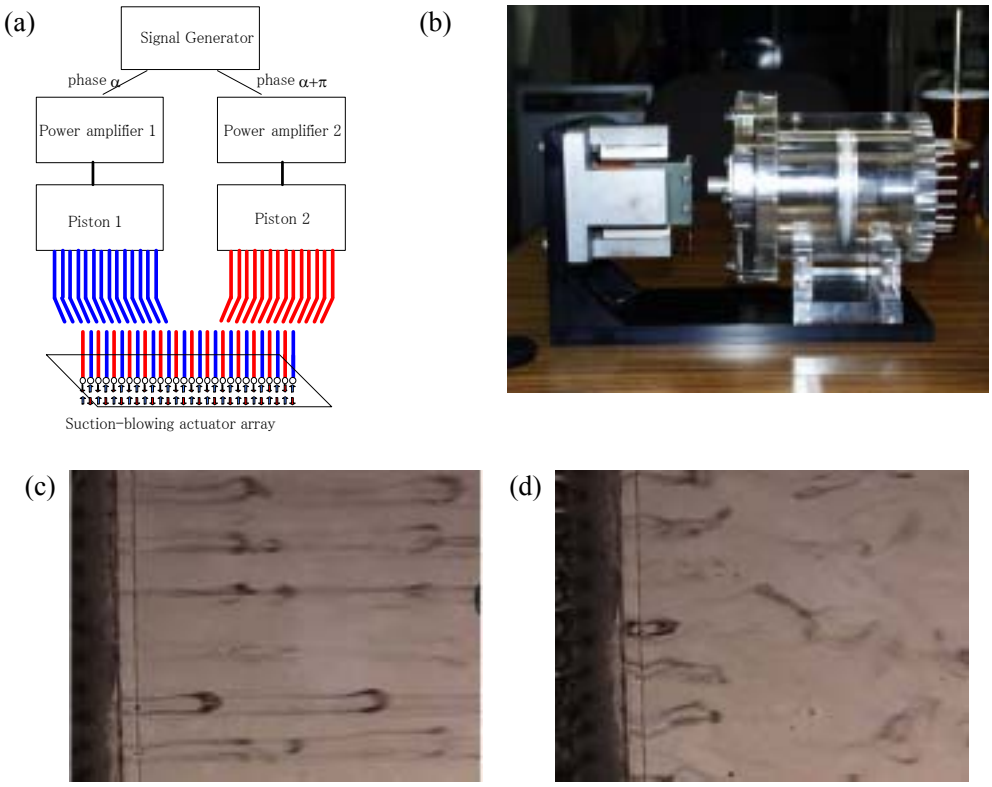


Figure 7 (a) Schematic drawing of suction-blowing actuator array system for a reactive turbulence control; (b) Picture of the piston system; (c) and (d) Two different flow patterns generated by the suction-blowing actuator array driven at the same frequency of $f_p$ = 5 Hz.

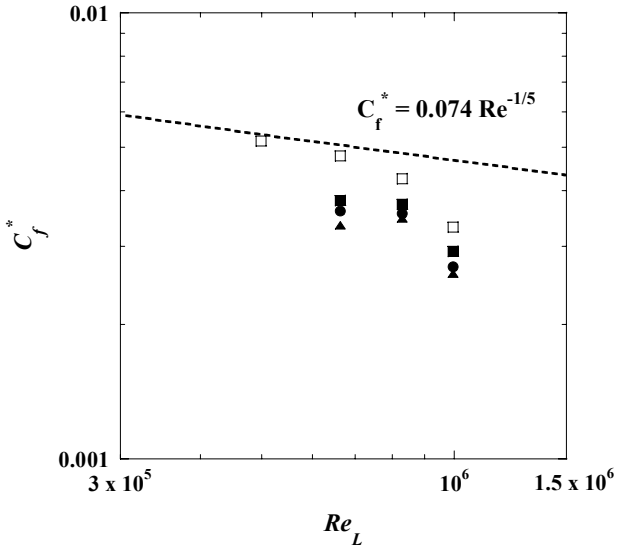


Figure 8 $C_f^*$ vs. $Re_L$ with the suction-blowing control in the water channel. The dotted line shows $C_f^* \sim Re_L^{-1/5}$. The open symbol (□) indicates $C_f^*$ without suction-blowing using the FBG system. The solid symbols indicate $C_f^*$ with suction-blowing using the FBG system, for $f_p$ = 1 Hz (■), 2 Hz (●), and 5 Hz (▲).